A biohybrid strategy for enabling photoredox catalysis with low-energy light

A Biohybrid Strategy for Enabling Photoredox Catalysis with Low Energy Light

Paul T. Cesana[1], Beryl X. Li[2], Samuel G. Shepard[3], Stephen I. Ting[2], Stephanie M. Hart[1], Courtney M. Olson[1], Jesus I. Martinez Alvarado[2], Minjung Son[1,4], Talia J. Steiman[2,5], Felix N. Castellano[3], Abigail G. Doyle[2], David W. C. MacMillan[2], and Gabriela S. Schlau-Cohen[1,*]

[1]Department of Chemistry, Massachusetts Institute of Technology, Cambridge, MA 02139, USA.

[2]Department of Chemistry, Princeton University, Princeton, NJ 08544, USA.

[3]Department of Chemistry, North Carolina State University, Raleigh, NC 27695, USA.

[4]Current address: Department of Chemistry, University of Wisconsin – Madison, Madison, WI 53706, USA.

[5]Current address: Snapdragon Chemistry Inc., Waltham, MA 02451, USA.

*Lead Contact: gssc@mit.edu (email).

SUMMARY

Natural systems drive the high-energy reactions of photosynthesis with efficient and broadband energy capture. Transition metal photocatalysts similarly convert light into chemical reactivity, yet suffer from light-limited operation and require blue-to-UV excitation. In photosynthesis, both light capture and reactivity have been optimized by separation into distinct sites. Inspired by this modular architecture, we synthesized a biohybrid photocatalyst by covalent attachment of the photosynthetic light-harvesting protein R-phycoerythrin (RPE) to the transition metal photocatalyst tris(2,2′-bipyridine)ruthenium(II) ($[Ru(bpy)_3]^{2+}$). Spectroscopic investigation found that absorbed photoenergy was efficiently funneled from RPE to $[Ru(bpy)_3]^{2+}$. The utility of the biohybrid photocatalyst was demonstrated via an increase in yields for a thiol-ene coupling reaction and a cysteinyl desulfurization reaction, including recovered reactivity at red wavelengths where $[Ru(bpy)_3]^{2+}$ alone does not absorb.

KEYWORDS

Photoredox catalysis, photosynthetic light harvesting, biohybrid, energy transfer

INTRODUCTION

Photoredox catalysis harnesses light energy to afford potent reactivity to a broad range of chemistries and substrates that are otherwise unreactive. Upon visible excitation, the photocatalyst is transformed into a high-energy reactive intermediate that can be used to promote challenging or previously elusive transformations.[1–4] The reactivity is most often ascribed to electron- or energy-transfer from long-lived triplet metal-to-ligand charge transfer (^{3}MLCT) states that generate potent reductants or oxidants.[5,6] For example, transition metal photoredox catalysts have been used for many carbon-carbon bond formations that have been instrumental in the development of pharmaceuticals, agrochemicals, and complex natural products.[7–13] Despite their catalytic utility, the charge transfer and other reactive states are limited by small absorption bandwidths (~100 nm) and low molar absorptivities (10^3-10^4 M^{-1} cm^{-1}), resulting in poor photon conversion efficiency.[3,14–17] Additionally, most transition metal photoredox catalysts require excitation at high photon energies where the effective absorbance is often further reduced by secondary catalysts, substrates or reagents that act as optical filters. The high energy excitation can also cause cellular damage and so has limited the biological applications of this powerful technology.[18–21]

Nature overcomes the poor light-harvesting ability of the charge transfer and similar reactive states with dedicated machinery to capture sunlight for photosynthesis.[22–27] Light-harvesting proteins absorb over large spectral bandwidths (~250 nm) with high molar absorptivities (~10^6 M^{-1} cm^{-1}), and then efficiently transfer this energy to sensitize neighboring proteins that contain the reactive site.[25–32] Inspired by the modularity found in biology, several types of photocatalysts have been produced that employ a similar approach.[33] Nanoparticles or small molecules were covalently attached to enzymes, and electron transfer between them has

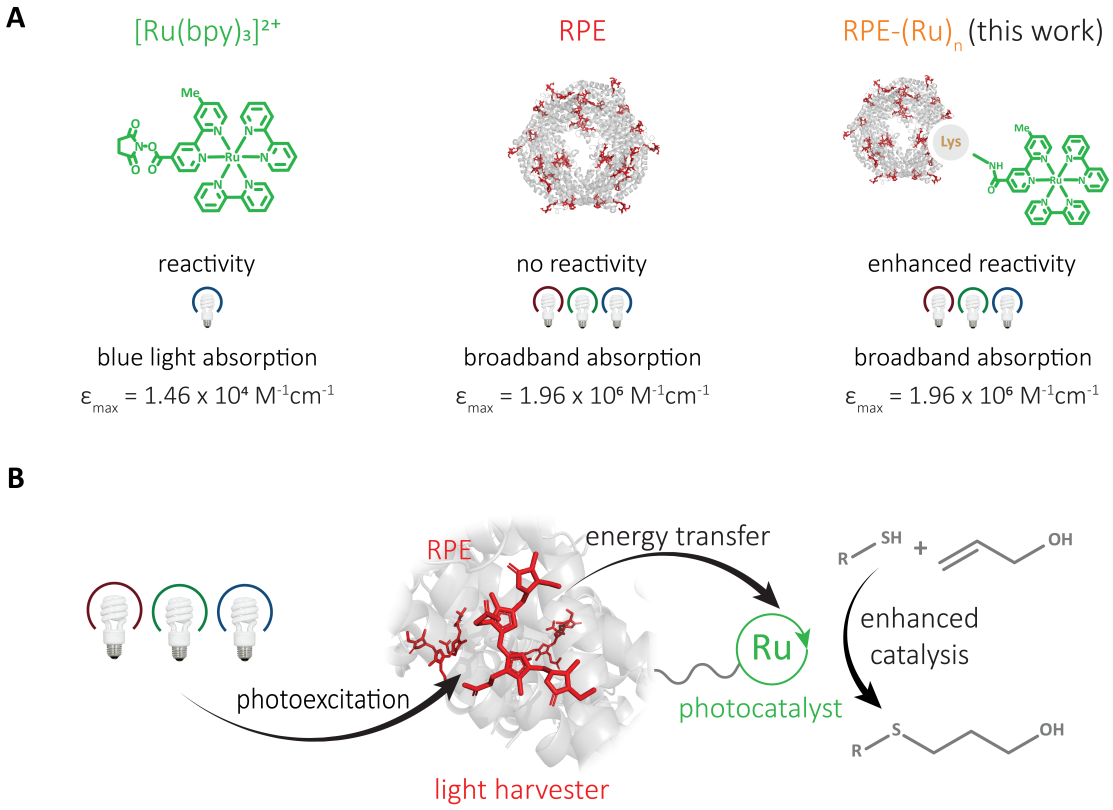

Figure 1: Components and concept of light-enhanced catalysis. (A) The small molecule photocatalyst, $[Ru(bpy)_3]^{2+}$ (green, left), conjugated to the photosynthetic light-harvesting protein, RPE (red, center), forms a biohybrid photocatalyst, RPE-$(Ru)_n$ (orange, right). The photocatalytic reactivity of $[Ru(bpy)_3]^{2+}$ and the light harvesting of RPE are combined in the RPE-$(Ru)_n$ biohybrid. (B) Schematic of RPE-$(Ru)_n$ photocatalysis in which photoexcitation of pigments (red, chemical structures in SI Figure S13) in RPE at any wavelength leads to energy transfer to $[Ru(bpy)_3]^{2+}$ (green), which can catalyze reactions.

been demonstrated.[34–43] However, the stringent distance dependence requirements and nonspecific reactivity of electron transfer create additional synthetic and operational challenges.[44–47] Energy transfer, which occurs over longer distances, was introduced by conjugating together transition metal photocatalysts with different excitation energies, which expanded their absorption window.[48–55] Despite the expanded absorption, the low extinction coefficients of the photocatalysts lead to light-limited activity under many conditions. The absorption range was also expanded into the low energy (near-infrared) region by direct excitation of the ^{3}MLCT state, and the utility of this scheme was demonstrated on a range of photoredox reactions.[56] However, the extremely low molar absorptivity (~10^2 M^{-1} cm^{-1}) of this

state limits its light-harvesting ability.[57–59] Upconversion of triplet states in a sensitizer/photocatalyst mixture was introduced as an alternative strategy to use near-infrared light, but with low photon conversion efficiency.[60–62] Finally, sensitization of a transition metal photoredox catalyst through energy transfer from light-harvesting ligands was demonstrated, but its impact on reactivity was not investigated.[63–65]

Here, we mimicked the design found in photosynthesis by conjugating the prototypical transition metal photocatalyst, tris(2,2′-bipyridine)ruthenium(II) ($[Ru(bpy)_3]^{2+}$), to the commercially-available, photosynthetic light-harvesting protein, R-phycoerythrin (RPE), from red algae (Figure 1). The resultant biohybrid, henceforth referred to as RPE-$(Ru)_n$, absorbed at wavelengths up to 630 nm and transferred energy from RPE to $[Ru(bpy)_3]^{2+}$. The energy capture provided by the light harvester enhanced catalytic yields by a factor of ten as compared to controls that lacked light harvesting for two representative reactions, a radical thiol-ene coupling and a cysteinyl desulfurization.

RESULTS AND DISCUSSION

Biohybrid Synthesis and Steady-State Characterization

Synthesis of the biohybrid construct shown in Figure 1A, right, was accomplished by taking advantage of the 72 surface-exposed lysine residues on RPE identified using Pymol (SI Section 3A). Conjugation of $[Ru(bpy)_3]^{2+}$ to the lysine side chains occurred readily upon treatment of RPE with a derivative of $[Ru(bpy)_3]^{2+}$ substituted with an *N*-hydroxysuccinimide ester (SI Figure S1). While conjugation to other amino acids is possible, the lysines are the most likely site due to the nucleophilicity of the amine group and their propensity for exterior positioning.[66,67] They are primarily evenly dispersed across the surface of the outer ring of the protein with two per subunit

on the ends of the cylinder-like structure (SI Figure S10), likely leading to stochastic decoration of the exterior of RPE with $[Ru(bpy)_3]^{2+}$. The NHS-ester derivative of $[Ru(bpy)_3]^{2+}$ was chosen as the catalyst because of its commercial availability and the historical prevalence of $[Ru(bpy)_3]^{2+}$. Purification by centrifugal filtration and FPLC afforded the hybrid in high purity (SI Section 1).

Intact mass spectrometry (MS) data was obtained for both free RPE and purified RPE-$(Ru)_n$ to confirm conjugation (SI Figure S7). RPE is a hexameric protein in which alpha (α) and beta (β) subunits form an $(\alpha\beta)_6$ quarternary structure. The MS of RPE showed the α and β subunits at masses of 18,889 Da and 20,308 Da, respectively, both in agreement with the

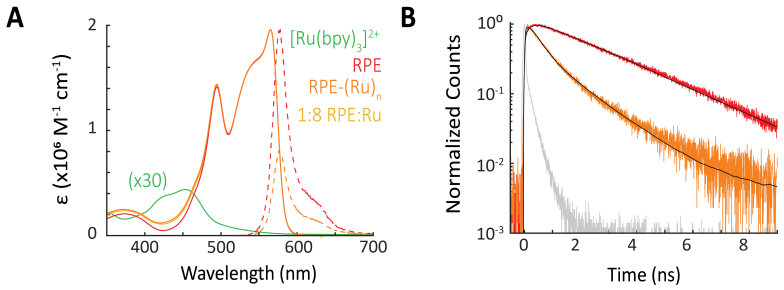

Figure 2: Steady-state absorption and time resolved fluorescence. (A) Absorption spectra of $[Ru(bpy)_3]^{2+}$, RPE, a mixture of RPE: $[Ru(bpy)_3]^{2+}$ in a 1:8 molar ratio, and RPE-$(Ru)_n$ with the relative fluorescence emission spectra of RPE and RPE-$(Ru)_n$. (B) Nanosecond fluorescence decays of RPE and RPE-$(Ru)_n$ with the IRF (gray).

literature.[68] Compared to free RPE, RPE-$(Ru)_n$ exhibited modifications of 610 Da in its mass spectrum, corresponding to the molecular weight of the $[Ru(bpy)_3]^{2+}$ catalyst. The α subunit showed equally abundant peaks (1:1:1) for no modification, one modification, and two modifications. The β subunit showed unequally abundant peaks (1:1:0.2) for no modification, one modification, and two modifications, respectively. A weighted average of this data was used to estimate that ten $[Ru(bpy)_3]^{2+}$ catalysts per one RPE were retained under the MS conditions.

The absorption and emission spectra of the conjugated hybrid are overlaid with its individual components in Figure 2A. RPE-$(Ru)_n$ had an absorption spectrum similar to the free

protein due to the significantly larger molar absorptivity coefficient (10^2-times) of RPE compared to $[Ru(bpy)_3]^{2+}$. The similar profile of the absorption spectra before and after conjugation also confirmed that integrity of the protein was maintained. As expected, RPE-$(Ru)_n$ showed additional absorbance in the region around the $[Ru(bpy)_3]^{2+}$ ^{1}MLCT states centered at 459 nm. Additionally, the peak in the RPE-$(Ru)_n$ spectrum corresponding to the energy of the $[Ru(bpy)_3]^{2+}$ bipyridine ligand $\pi \rightarrow \pi^*$ transition (285 nm) increased in intensity relative to the free protein (SI Figure S8). Finally, the sum of the component spectra matched well with the spectrum of the purified RPE-$(Ru)_n$ with a 1:8 ratio, similar to the results from MS and confirming conjugation (SI Figure S8).

The steady state fluorescence emission spectra of free RPE and RPE-$(Ru)_n$ are also

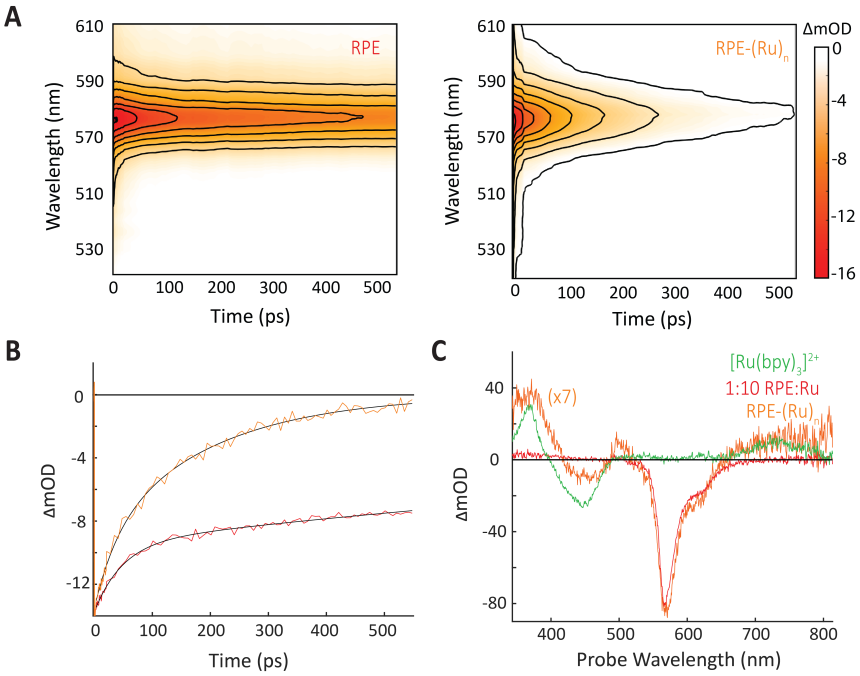

Figure 3: Transient absorption of RPE-Ru biohybrid. (A) Ultrafast transient absorption spectra of RPE (left) and RPE-$(Ru)_n$ (right). The ground state bleach shows a faster decrease for the hybrid as compared to the free protein. (B) Kinetic traces of both samples at 570 nm. (C) Nanosecond transient absorption spectra of $[Ru(bpy)_3]^{2+}$, RPE-$(Ru)_n$, and a mixture of RPE and Ru.

shown. The spectral profiles were essentially the same due to the much lower level of photoluminescence emission from $[Ru(bpy)_3]^{2+}$. The integrated fluorescence intensity decreased by ~60% for RPE-$(Ru)_n$ compared to RPE, providing further evidence of successful conjugation and indicating the presence of energy transfer.

Characterization of the Excited-State Dynamics

Time-resolved spectroscopy was used to characterize the photophysics of the biohybrid. The fluorescence lifetime was measured for both the free protein and biohybrid structure. The RPE fluorescence emission (Figure 2B) showed a monoexponential decay with a timescale of 2.63 ns, in agreement with literature values of 2.3-3.1 ns.[28,29] In contrast, the RPE-$(Ru)_n$ emission showed a multi-exponential decay profile, which was best fit with a tri-exponential function. The two fast timescales were ~0.039 ns and ~0.368 ns, each with an amplitude of ~40%. The slower timescale was 1.70 ns. The average lifetime was 0.384 ns, which gave an overall energy transfer efficiency of 85%. The fitting parameters for all samples are summarized in SI Tables S2 and S3.As discussed above, although each RPE-$(Ru)_n$ contains on average ten $[Ru(bpy)_3]^{2+}$, the sample is a heterogeneous mixture with $[Ru(bpy)_3]^{2+}$ attached to RPE in a variety of stoichiometries and conjugation sites. We assign the two fast timescales to uphill energy transfer from RPE to $[Ru(bpy)_3]^{2+}$ in RPE-$(Ru)_n$ with a large number of conjugated $[Ru(bpy)_3]^{2+}$ and/or $[Ru(bpy)_3]^{2+}$ well-positioned for energy transfer. Consistent with this assignment, the timescale of energy transfer for RPE-$(Ru)_n$ with ten $[Ru(bpy)_3]^{2+}$ was calculated to be 0.409 ns using Förster theory (SI Section 3). These calculations also predict an 78% energy transfer efficiency, close to the experimental value. Förster energy transfer is governed by the spectral overlap and distance between the donor and acceptor. Due to the small spectral overlap, each energy transfer pathway is inefficient. However, they give an overall high energy transfer efficiency from the combined

contributions of the ten energy transfer pathways from RPE to $[Ru(bpy)_3]^{2+}$ (SI Section 3B). Despite the uphill nature of the energy transfer step, rapid trapping of the excitation by intersystem crossing on $[Ru(bpy)_3]^{2+}$ likely limited back transfer. We assign the slow timescale to energy transfer in the small population of RPE-$(Ru)_n$ only bearing conjugated $[Ru(bpy)_3]^{2+}$ that are poorly positioned for energy transfer.

Transient absorption (TA) spectroscopy was used to monitor the excited-state dynamics, including transitions into non-emissive states. To probe the photophysical pathways with high temporal resolution, ultrafast TA measurements were performed on both RPE and RPE-$(Ru)_n$ with excitation at 540 nm, which overlaps with the RPE absorption peak. For free RPE (Figure 3A, left), initial excitation gave rise to a ground state bleach (GSB)/stimulated emission (SE) signal across the absorption spectrum. As shown in Figure 3B, the GSB/SE signal at the low-energy state of RPE decayed on 54 ps and 2.2 ns (1.56 ns average) timescales, similar to previously observed values.[28] For RPE-$(Ru)_n$ (Figure 3A, right), the GSB/SE signal decayed more quickly across the spectrum, likely as a result of energy transfer to $[Ru(bpy)_3]^{2+}$. As shown in Figure 3B, the signal at the low energy state decayed on 36 ps and 170 ps (137 ps average lifetime) timescales, consistent with the fluorescence lifetime measurements and calculations of the energy transfer timescale from RPE to $[Ru(bpy)_3]^{2+}$.

To more directly probe $[Ru(bpy)_3]^{2+}$ sensitization upon RPE excitation, we employed nanosecond TA spectroscopy on RPE-$(Ru)_n$, $[Ru(bpy)_3]^{2+}$, and an unconjugated mixture of RPE and $[Ru(bpy)_3]^{2+}$. The prompt transient spectra are shown for all three samples in Figure 3C. For $[Ru(bpy)_3]^{2+}$ excited at 450 nm, the characteristic GSB at 450 nm and ESA at 380 nm were observed, consistent with previous reports.[69] For the unconjugated mixture, after excitation of RPE at 540 nm, a component of the RPE GSB/SE persisted while spectral features of excited

$[Ru(bpy)_3]^{2+}$ were absent. For the RPE-$(Ru)_n$ conjugate, a similar GSB/SE component was present in the RPE spectral region, but the spectral features of $[Ru(bpy)_3]^{2+}$ also appeared, signaling successful energy transfer to the photocatalyst. Excitation further toward the red, at 580 nm, also demonstrated energy transfer to the photocatalyst (SI Figure S22). Energy transfer is expected to populate the charge transfer bands of $[Ru(bpy)_3]^{2+}$ almost exclusively for excitation wavelengths above 500 nm, as the catalytically deleterious triplet metal centered state is higher in energy.[55,70] Although these experiments provide spectral evidence that energy transfer occurs, the signals of energy transfer appear within the 8 ns instrument response function, so the timescale of energy transfer cannot be discerned from this experiment (SI Section 4C). These results do, however, provide direct experimental evidence of the assignment to energy transfer, as electron transfer would have resulted in the spectra of the oxidized or reduced form of $[Ru(bpy)_3]^{2+}$ in the RPE-$(Ru)_n$ sample.[44]

Demonstration of Enhanced Catalysis Using the Biohybrid

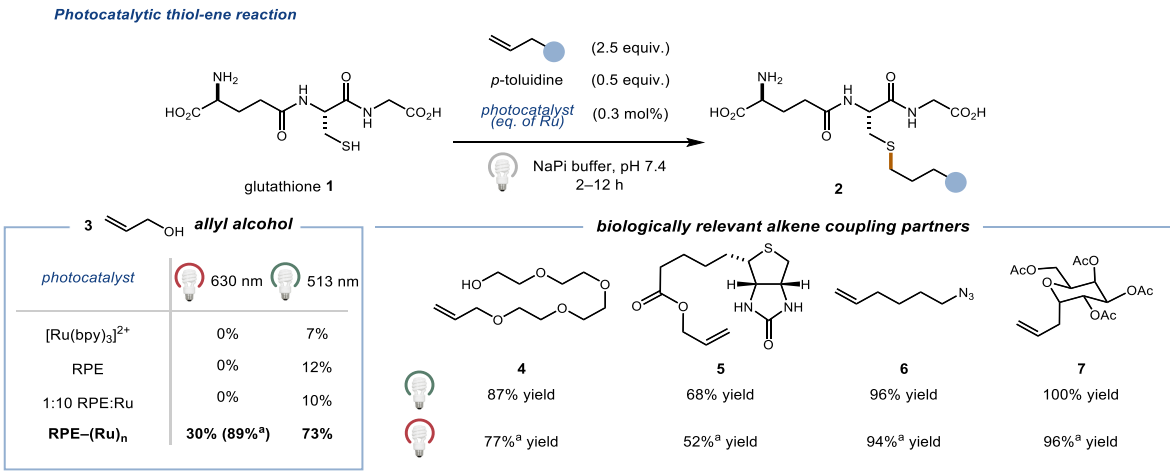

Figure 4. Photocatalytic radical thiol-ene reaction. RPE-$(Ru)_n$ enables or enhances yields at red and green wavelengths. Reaction times are 2 h except where denoted. [a]12 h reaction time. Note: "eq. of Ru" refers to the fact that all reactions were performed with catalyst loadings normalized to $[Ru(bpy)_3]^{2+}$.

To establish the catalytic ability of RPE-$(Ru)_n$, we assessed product yields for two radical initiation reactions previously reported in literature, a thiol-ene coupling and a cysteinyl desulfurization.[71,72] The goal of this proof-of-concept study is to identify an enhancement in catalytic performance and, for radical chain reactions, differences in the photodriven initiator formation can be easily observed in the final product yields. While the sequential nature of the propagation means that the improvement in the photodriven process cannot be straightforwardly quantified, these reactions allow for clear qualitative comparison of yields. Performance in the presence of RPE-$(Ru)_n$ was compared to $[Ru(bpy)_3]^{2+}$, RPE, and an unconjugated mixture of RPE and $[Ru(bpy)_3]^{2+}$ as controls at three LED wavelengths (blue, 459 nm; green, 513 nm; red, 630 nm). Full experimental details, including all yields, substrates, and product NMR characterization are included in the SI Sections 5 and 6.

We first investigated the effectiveness of RPE-$(Ru)_n$ in the thiol-ene reaction, a widely adopted bioconjugation strategy extended to photoredox catalysis by Yoon and co-workers.[71,73,74]

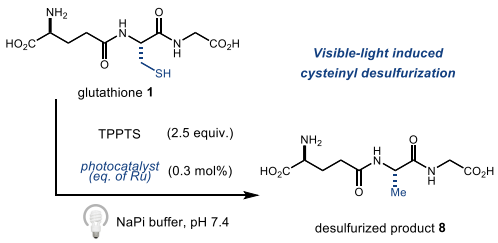

photocatalyst	630 nm [a]	513 nm [b]	459 nm [b]
$[Ru(bpy)_3]^{2+}$	0%	0%	85% [c]
RPE	0%	0%	–
1:10 RPE:Ru	0%	0%	–
RPE–$(Ru)_n$	**78%**	**100%**	–
RPE–$(Ru)_n$ reuse	**65%**	**83%**	–

Figure 5. Visible-light induced cysteinyl desulfurization. [a]36 h irradiation, [b]12 h irradiation, [c]Literature-reported yield.[72] TPPTS: 3,3′,3″-phosphanetriyltris trisodium salt.

Relative to small molecule $[Ru(bpy)_3]^{2+}$, coupling of glutathione (**1**) and allyl alcohol (**3**) under RPE-$(Ru)_n$ catalysis presented improved yields under red, green, and blue light irradiation (Figure 4, SI Section 5). Most notably, RPE-$(Ru)_n$ afforded product **2** in 89% yield under red light irradiation, whereas no product formation was observed with $[Ru(bpy)_3]^{2+}$. Under green irradiation, which corresponds to the maximum of the RPE absorbance, **2** was generated in ~10% yield with $[Ru(bpy)_3]^{2+}$ alone and with the unconjugated $[Ru(bpy)_3]^{2+}$ and RPE mixture. By contrast, RPE-$(Ru)_n$ catalyzed the reaction in 70% yield. The yields with RPE-$(Ru)_n$ under both green and red irradiation were higher than the yield with $[Ru(bpy)_3]^{2+}$ alone under blue irradiation at the maximum of its absorbance (10%, in agreement with previous literature reports[74]). To demonstrate the generality of the observed enhancement, four additional substrates (**4**-**7**) were evaluated. In all cases, product yields under green or red irradiation surpassed yields achieved by $[Ru(bpy)_3]^{2+}$ alone or by the unconjugated $[Ru(bpy)_3]^{2+}$/RPE mixture, even reaching quantitative yields for glycosylation (**7**). The ability to catalyze the reaction at red wavelengths is afforded by uphill energy transfer utilizing thermal energy to account for differences in activation energy (SI Section 3C).[75,76] Furthermore, both product yields and photostability of RPE-$(Ru)_n$ increased under low irradiance, indicating that optimal operation may require the photon absorption rate to be empirically matched to the catalytic cycle. These results demonstrate the ability of RPE-$(Ru)_n$ to improve catalytic performance and enable operation under irradiation at any visible wavelength.

To determine the versatility of our RPE-$(Ru)_n$, we also investigated its performance in a cysteinyl desulfurization method developed by Guo and co-workers in 2016.[72] The original reaction, which employs 5 mol% of $[Ru(bpy)_3]^{2+}$, converted glutathione (**1**) to product **8** with 85% yield under blue light irradiation. With our RPE-$(Ru)_n$ biohybrid, the desulfurization proceeds

with similarly high efficiencies under red or green light irradiation (78% and 100%, respectively) using 0.3 mol% of the catalyst. Notably, control reactions with $[Ru(bpy)_3]^{2+}$, RPE, or the unconjugated mixture of the two species showed no reactivity across both irradiation wavelengths (Figure 5). The reduced catalyst loading of 0.3 mol% under conditions relevant to this manuscript compared to the previously reported value of 5 mol% also demonstrates the synthetic competency of the biohybrid.[72] Furthermore, the large RPE appendage with a mass of 240 kDa allowed for facile catalyst recovery through centrifugal filtration with a 50 kDa MWCO filter. Biohybrid reusability was screened by resubjecting RPE-$(Ru)_n$ to fresh reagents, affording 83% yield under green light irradiation and 65% yield under red light irradiation. Thus, along with improvements to product yields, the biohybrid serves as a homogeneous catalyst with the key reusability advantage of heterogeneous catalysis.[77,78]

CONCLUSION

A biohybrid catalyst consisting of the photosynthetic light-harvesting protein RPE and multiple conjugated $[Ru(bpy)_3]^{2+}$ photocatalysts has been synthesized, characterized, and shown to improve catalytic efficiency. Energy transfer from RPE to $[Ru(bpy)_3]^{2+}$ improved yields and enabled reactivity even at red wavelengths. The biohybrid photocatalyst is also environmentally sustainable as it operates in aqueous conditions, exhibits activity under low-energy irradiation, and is easily reused. These initial demonstrations lay the groundwork for the development of photocatalysts with distinct light harvesting and reactive components as seen in photosynthesis, which, as illustrated here, allows robust and reliable reactivity.

EXPERIMENTAL PROCEDURES

Resource Availability

Lead Contact

Further information and requests for resources should be directed to and will be fulfilled by the lead contact, Gabriela S. Schlau-Cohen (gssc@mit.edu).

Materials Availability

All materials generated in this study are available from the lead contact upon request.

Data and Code Availability

Data and code generated during this study are available from the lead contact upon request.

Sample Preparation

R-phycoerythrin (RPE; Agilent, Cat. No. PB-32) was dialyzed against phosphate buffer (0.1 M sodium phosphate, pH = 7.5, filter sterilized and degassed) and refrigerated until needed. Bis(2,2′-bipyridine)-4′-methyl-4-carboxybipyridine-ruthenium (II) *N*-succinimidyl ester bis(hexafluorophosphate) ($[Ru(bpy)_3]^{2+}$-NHS ester, Sigma-Aldrich Cat. No. 96631) and dimethyl sulfoxide (DMSO) were used as received. Bioconjugation of the $[Ru(bpy)_3]^{2+}$-NHS ester to RPE was performed by reacting R-phycoerythrin (250 μL of 1 mg/mL in phosphate buffer) with $[Ru(bpy)_3]^{2+}$-NHS ester (50 μL of 20 mg/mL in DMSO, ~950x molar excess of catalyst).[79] Multiple small-scale (300 μL) reactions were performed in parallel to allow $[Ru(bpy)_3]^{2+}$-NHS ester to easily mix with phycobiliproteins without hydrolysis of the NHS ester. The reaction mixtures were placed on an incubator shaker (1100 RPM) at room temperature for 1 h. After incubation, the small-scale reaction mixtures were combined, placed into a 50 kDa molecular weight cut-off centrifugal filter (Millipore, Cat. No. UFC9050) and centrifuged at 4° and 4000 rpm (3220 rcf) for 15-20 min. Further purification was performed using fast protein liquid chromatography (FPLC) with a NGC chromatography system (Bio-Rad) on a Superose® 6

10/300 GL column (Cytiva Life Sciences) at a flow rate of 0.5-0.75 mL/min at 4° in phosphate buffer. Fractions of the peak eluting at 16.2 mL for RPE were collected and centrifuge concentrated using the same parameters as described above. All reactions and spectroscopic studies were performed in phosphate buffer (0.1 M sodium phosphate, pH = 7.5, filter sterilized and degassed). Further details on conjugation and purification are provided in the SI section 1.

Steady-state Absorption and Fluorescence Measurements

Linear absorbance spectra were acquired using a Shimadzu UV-2401PC spectrophotometer. Fluorescence emission spectra were obtained using a Varian Cary Eclipse with 565 nm excitation at the maximum absorbance of RPE.

Fluorescence Lifetime Measurements

Fluorescence lifetime measurements were performed using a supercontinuum generated in a nonlinear photonic crystal fiber (FemtoWhite 800, NKT photonics) pumped by a Ti:sapphire oscillation (Mai Tai, Spectra Physics). Full details on the laser setup are in the SI Section 4. The excitation wavelength was selected using a 550 nm, 15 nm FWHM bandpass filter (Chroma Technology Corp ET550/15x) and the emission wavelength was selected using a 580 nm, 10 nm FWHM bandpass filter (Thor Labs FB580-10). The excitation laser pulse was focused on a 1 cm x 2 mm pathlength quartz cuvette (Hellma Analytics 108.002F-QS) to a spot size of 0.66 μm^2 and with a pulse energy of 0.027 nJ per pulse. The instrument response function (IRF) was measured using a scatter solution containing a 1:100 v:v mixture of HS-40 colloidal silica (Sigma-Aldrich) and phosphate buffer with a width of 75-95 ps (FWHM). Fluorescence lifetime decay curves were individually fitted to a mono- or tri-exponential function using iterative reconvolution with the IRF.

Intact Mass Spectrometry (Intact MS)

RPE and RPE-$(Ru)_n$ were loaded onto a Thermo MAbPac RP column using an Agilent1100 HPLC system. Further details on chromatography elution parameters can be found in SI Section 2A. MS data was acquired in profile mode with a Thermo QE mass spectrometer at 17,000 resolution, and analyzed using ThermoBioPharma Finder™ 3.2 ReSpect with default settings.

Transient Absorption (TA) Studies

Femtosecond transient absorption studies were conducted using a broadband white light source, the complete details of which are described in SI Section 4B. Briefly, pulses were obtained using the output of a Ti:sapphire regenerative amplifier (Coherent Libra, 5 kHz, 1.1 mJ, 40 fs pulse, λ_c=800 nm). White light was generated using an argon gas chamber (20 psi) and filtered for a center wavelength of 540 nm. Spectra were collected by measuring the probe laser for each pulse using a line CCD (e2v) and chopping the pump laser at 2.5 kHz.[80] Samples were prepared at an OD of 0.3 in a 1 mm path cuvette, flowed with a peristaltic pump to prevent photodegradation and re-excitation, and chilled to 8° C throughout the measurement. Linear absorption spectra were collected before and after TA to confirm sample integrity was retained.

Nanosecond transient absorption spectra were acquired on an Edinburgh Instruments LP 920 spectrometer outfitted with a liquid nitrogen equipped temperature controller (Unisoku CoolSpeK). Samples were excited using the output of a tunable OPO (Opotek Vibrant 355) operating at 1 Hz. The excitation source was kept to less than 2.5 mJ/pulse (~5 mJ/cm^2). The probe source of the LP 920 (a xenon arc lamp) was also filtered through two long-pass filters (290 nm and 320 nm) to prevent the UV component of the probe light from degrading the sample. Samples were prepared in quartz 1 cm cuvettes with aqueous phosphate buffer solutions, stirred, and kept at 8 °C for the duration of the experiment. To capture the transient absorption signals for the bound ruthenium chromophores, which have small excited-state-induced changes

in molar absorptivity relative to the protein, sample absorbances of 0.6-0.9 at 565 nm were used. The pulse duration was 8 ns (see note in final paragraph of SI Section 4C).

Synthetic Reactions

Thiol-ene coupling[71] and cysteinyl desulfurization[72] reactions were performed as described in the literature, with modifications due to the requirements of RPE-$(Ru)_n$. The reactions were performed in phosphate buffer, at the reduced scale dictated by the protein, without agitation to prevent aggregation, and with reduced light intensity due to the greater absorbance of the protein. Reactions were replicated and screened at three LED illuminations (blue, green, red) for the $[Ru(bpy)_3]^{2+}$, RPE, RPE-$(Ru)_n$, and an unconjugated mixture of the two components, and examined for enhanced yields using ^1H NMR against an external standard. Quantum yield measurements were performed on both test reactions using ferrioxalate actinometry. We also screened RPE-$(Ru)_n$ reusability after recovery via size-exclusion centrifugal filtration. Full experimental details are described in the SI Sections 5 and 6.

SUPPLEMENTAL INFORMATION

Details on bioconjugation, purification, spectroscopic measurements, calculations of RPE-$(Ru)_n$ energy transfer rate, and synthetic reactions.

ACKNOWLEDGMENTS

This work was supported as part of BioLEC, an Energy Frontier Research Center funded by the U.S. Department of Energy, Office of Science under Award # DE-SC0019370. The authors acknowledge Antonius Koller of the Koch Institute for Integrative Cancer Research at MIT for the Intact MS measurements.

AUTHOR CONTRIBUTIONS

Conceptualization, P.T.C., B.X.L., C.M.O., M.S., T.J.S., F.N.C., A.G.D., D.W.C.M., and G.S.S-C.; Resources, P.T.C., C.M.O., S.M.H., M.S., and T.J.S.; Investigation, P.T.C., S.M.H., S.G.S., B.X.L., S.I.T., and J.I.M.A.; Writing-Original Draft, P.T.C., B.X.L., and G.S.S-C.; Writing-Review and Editing, P.T.C., B.X.L., S.I.T., S.G.S., J.I.M.A., F.N.C., A.G.D., D.W.C.M., and G.S.S-C.; Funding Acquisition, F.N.C., A.G.D., D.W.C.M., and G.S.S-C.; Supervision, F.N.C., A.G.D., D.W.C.M., and G.S.S-C.

DECLARATION OF INTERESTS

The authors declare no competing interests.

REFERENCES

1. Douglas, J.J., Sevrin, M.J., and Stephenson, C.R.J. (2016). Visible Light Photocatalysis: Applications and New Disconnections in the Synthesis of Pharmaceutical Agents. Org. Process Res. Dev. *20*, 1134–1147. 10.1021/acs.oprd.6b00125.
2. Fagnoni, M., Dondi, D., Ravelli, D., and Albini, A. (2007). Photocatalysis for the formation of the C-C bond. Chem. Rev. *107*, 2725–2756. 10.1021/cr068352x.
3. Osterloh, F.E. (2017). Photocatalysis versus Photosynthesis: A Sensitivity Analysis of Devices for Solar Energy Conversion and Chemical Transformations. ACS Energy Lett. *2*, 445–453. 10.1021/acsenergylett.6b00665.
4. Zhu, S., and Wang, D. (2017). Photocatalysis: Basic principles, diverse forms of implementations and emerging scientific opportunities. Adv. Energy Mater. *7*, 1700841.

10.1002/aenm.201700841.

5. Turro, N.J. (1977). Energy Transfer Processes. Pure Appl. Chem. *49*, 405–429. https://doi.org/10.7916/D8RV0V0T.

6. Kavarnos, G.J., and Turro, N.J. (1986). Photosensitization by reversible electron transfer: Theories, experimental evidence, and examples. Chem. Rev. *86*, 401–449. https://doi.org/10.1021/cr00072a005.

7. Prier, C.K., Rankic, D.A., and MacMillan, D.W.C. (2013). Visible light photoredox catalysis with transition metal complexes: Applications in organic synthesis. Chem. Rev. *113*, 5322–5363. 10.1021/cr300503r.

8. Cheng, W.M., and Shang, R. (2020). Transition Metal-Catalyzed Organic Reactions under Visible Light: Recent Developments and Future Perspectives. ACS Catal. *10*, 9170–9196. 10.1021/acscatal.0c01979.

9. Shaw, M.H., Twilton, J., and MacMillan, D.W.C. (2016). Photoredox Catalysis in Organic Chemistry. J. Org. Chem. *81*, 6898–6926. 10.1021/acs.joc.6b01449.

10. Xuan, J., and Xiao, W.J. (2012). Visible-light photoredox catalysis. Angew. Chemie - Int. Ed. *51*, 6828–6838. 10.1002/anie.201200223.

11. Romero, N.A., and Nicewicz, D.A. (2016). Organic Photoredox Catalysis. Chem. Rev. *116*, 10075–10166. 10.1021/acs.chemrev.6b00057.

12. Tucker, J.W., and Stephenson, C.R.J. (2012). Shining light on photoredox catalysis: Theory and synthetic applications. J. Org. Chem. *77*, 1617–1622. 10.1021/jo202538x.

13. Sayre, H.J., Tian, L., Son, M., Hart, S.M., Liu, X., Arias-Rotondo, D.M., Rand, B.P., Schlau-Cohen, G.S., and Scholes, G.D. (2021). Solar fuels and feedstocks: The quest for renewable black gold. Energy Environ. Sci. *14*, 1402–1419. 10.1039/d0ee03300f.

14. McCusker, J.K. (2019). Electronic structure in the transition metal block and its implications for light harvesting. Science. *363*, 484–488. 10.1126/science.aav9104.

15. Shaw, G.B., Styers-Barnett, D.J., Gannon, E.Z., Granger, J.C., and Papanikolas, J.M. (2004). Interligand electron transfer dynamics in [Os(bpy) 3] 2+: Exploring the excited state potential surfaces with femtosecond spectroscopy. J. Phys. Chem. A *108*, 4998–5006. 10.1021/jp0363850.

16. Dongare, P., Myron, B.D.B., Wang, L., Thompson, D.W., and Meyer, T.J. (2017). [Ru(bpy)3]2+ revisited. Is it localized or delocalized? How does it decay? Coord. Chem. Rev. *345*, 86–107. 10.1016/j.ccr.2017.03.009.

17. McCusker, J.K. (2003). Femtosecond Absorption Spectroscopy of Transition Metal Charge-Transfer Complexes. Acc. Chem. Res. *36*, 876–887. 10.1021/ar030111d.

18. Li, P., Terrett, J.A., and Zbieg, J.R. (2020). Visible-Light Photocatalysis as an Enabling Technology for Drug Discovery: A Paradigm Shift for Chemical Reactivity. ACS Med. Chem. Lett. *11*, 2120–2130. 10.1021/acsmedchemlett.0c00436.

19. Weng, Y., Song, C., Chiang, C.W., and Lei, A. (2020). Single electron transfer-based peptide/protein bioconjugations driven by biocompatible energy input. Commun. Chem. *3*, 1–11. 10.1038/s42004-020-00413-x.

20. Bottecchia, C., and Noël, T. (2019). Photocatalytic Modification of Amino Acids, Peptides, and Proteins. Chem. - A Eur. J. *25*, 26–42. 10.1002/chem.201803074.

21. Ryu, K.A., Kaszuba, C.M., Bissonnette, N.B., Oslund, R.C., and Fadeyi, O.O. (2021). Interrogating biological systems using visible-light-powered catalysis. Nat. Rev. Chem. *5*, 322–337. 10.1038/s41570-021-00265-6.

22. Mirkovic, T., Ostroumov, E.E., Anna, J.M., Van Grondelle, R., Govindjee, and Scholes,

G.D. (2017). Light absorption and energy transfer in the antenna complexes of photosynthetic organisms. Chem. Rev. *117*, 249–293. 10.1021/acs.chemrev.6b00002.

23. Frank, H.A., and Cogdell, R.J. (2012). Light capture in photosynthesis (Elsevier Ltd.).

24. Watanabe, M., and Ikeuchi, M. (2013). Phycobilisome: Architecture of a light-harvesting supercomplex. Photosynth. Res. *116*, 265–276. 10.1007/s11120-013-9905-3.

25. Ma, J., You, X., Sun, S., Wang, X., Qin, S., and Sui, S.F. (2020). Structural basis of energy transfer in Porphyridium purpureum phycobilisome. Nature *579*, 146–151. 10.1038/s41586-020-2020-7.

26. Zhang, J., Ma, J., Liu, D., Qin, S., Sun, S., Zhao, J., and Sui, S.F. (2017). Structure of phycobilisome from the red alga Griffithsia pacifica. Nature *551*, 57–63. 10.1038/nature24278.

27. Saer, R.G., and Blankenship, R.E. (2017). Light harvesting in phototrophic bacteria: Structure and function. Biochem. J. *474*, 2107–2131. 10.1042/BCJ20160753.

28. Chen, H., Dang, W., Xie, J., Zhao, J., and Weng, Y. (2012). Ultrafast energy transfer pathways in R-phycoerythrin from Polysiphonia urceolata. Photosynth. Res. *111*, 81–86. 10.1007/s11120-011-9708-3.

29. Gaigalas, A., Gallagher, T., Cole, K.D., Singh, T., Wang, L., and Zhang, Y.-Z. (2006). A Multistate Model for the Fluorescence Response of R-Phycoerythrin. Photochem. Photobiol. *82*, 635. 10.1562/2005-05-26-ra-544.

30. Seibert, M., and Connolly, J.S. (1984). Fluorescence Properties of C-Phycocyanin Isolated From a Thermophilic Cyanobacterium. Photochem. Photobiol. *40*, 267–271. 10.1111/j.1751-1097.1984.tb04585.x.

31. O'Carra, P., O'Heocha, C., and Carrol, D.M. (1964). Spectral Properties of the

Phycobilins. II. Phycoerythrobilin. Biochemistry *3*, 1343–1350. 10.1021/bi00897a026.

32. MacColl, R., and Guard-Frier, D. (1987). Phycobiliproteins 2018 Reiss. (CRC Press).

33. Mulfort, K.L., and Utschig, L.M. (2016). Modular Homogeneous Chromophore-Catalyst Assemblies. Acc. Chem. Res. *49*, 835–843. 10.1021/acs.accounts.5b00539.

34. Soltau, S.R., Dahlberg, P.D., Niklas, J., Poluektov, O.G., Mulfort, K.L., and Utschig, L.M. (2016). Ru-protein-Co biohybrids designed for solar hydrogen production: understanding electron transfer pathways related to photocatalytic function. Chem. Sci. *7*, 7068–7078. 10.1039/C6SC03121H.

35. Kathiravan, A., Chandramohan, M., Renganathan, R., and Sekar, S. (2009). Photoinduced electron transfer from phycoerythrin to colloidal metal semiconductor nanoparticles. Spectrochim Acta A Mol Biomol Spectrosc. *72*, 496–501. 10.1016/j.saa.2008.10.021.

36. Proppe, A.H., Li, Y.C., Aspuru-Guzik, A., Berlinguette, C.P., Chang, C.J., Cogdell, R., Doyle, A.G., Flick, J., Gabor, N.M., van Grondelle, R., et al. (2020). Bioinspiration in light harvesting and catalysis. Nat. Rev. Mater. *5*, 828–846. 10.1038/s41578-020-0222-0.

37. Grimme, R.A., Lubner, C.E., Bryant, D.A., and Golbeck, J.H. (2008). Photosystem I/molecular wire/metal nanoparticle bioconjugates for the photocatalytic production of H2. J. Am. Chem. Soc. *130*, 6308–6309. 10.1021/ja800923y.

38. Edwards, E.H., and Bren, K.L. (2020). Light-driven catalysis with engineered enzymes and biomimetic systems. Biotechnol. Appl. Biochem. *67*, 463–483. 10.1002/bab.1976.

39. Brown, K.A., Wilker, M.B., Boehm, M., Hamby, H., Dukovic, G., and King, P.W. (2016). Photocatalytic Regeneration of Nicotinamide Cofactors by Quantum Dot-Enzyme Biohybrid Complexes. ACS Catal. *6*, 2201–2204. 10.1021/acscatal.5b02850.

40. Herman, L., Ghosh, S., Defrancq, E., and Mesmaeker, A.K. De (2008). Ru(II) complexes

and light: Molecular tools for biomolecules. J. Phys. Org. Chem. *21*, 670–681. 10.1002/poc.1355.

41. Schwochert, T.D., Cruz, C.L., Watters, J.W., Reynolds, E.W., Nicewicz, D.A., and Brustad, E.M. (2020). Design and Evaluation of Artificial Hybrid Photoredox Biocatalysts. ChemBioChem *21*, 3146–3150. 10.1002/cbic.202000362.

42. Utterback, J.K., Ruzicka, J.L., Keller, H.R., Pellows, L.M., and Dukovic, G. (2020). Electron transfer from semiconductor nanocrystals to redox enzymes. Annu. Rev. Phys. Chem. *71*, 335–359. 10.1146/annurev-physchem-050317-014232.

43. Wilker, M.B., Shinopoulos, K.E., Brown, K.A., Mulder, D.W., King, P.W., and Dukovic, G. (2014). Electron transfer kinetics in CdS nanorod-[FeFe]-hydrogenase complexes and implications for photochemical H2 generation. J. Am. Chem. Soc. *136*, 4316–4324. 10.1021/ja413001p.

44. Arias-Rotondo, D.M., and McCusker, J.K. (2016). The photophysics of photoredox catalysis: A roadmap for catalyst design. Chem. Soc. Rev. *45*, 5803–5820. 10.1039/c6cs00526h.

45. Rupp, M., Auvray, T., Rousset, E., Mercier, G.M., Marvaud, V., Kurth, D.G., and Hanan, G.S. (2019). Photocatalytic Hydrogen Evolution Driven by a Heteroleptic Ruthenium(II) Bis(terpyridine) Complex. Inorg. Chem. *58*, 9127–9134. 10.1021/acs.inorgchem.9b00698.

46. Ma, B., Chen, G., Fave, C., Chen, L., Kuriki, R., Maeda, K., Ishitani, O., Lau, T.-C., Bonin, J., and Robert, M. (2020). Efficient Visible-Light-Driven CO 2 Reduction by a Cobalt Molecular Catalyst Covalently Linked to Mesoporous Carbon Nitride. J. Am. Chem. Soc. *142*, 6188–6195. 10.1021/jacs.9b13930.

47. Scandola, F., Indelli, M.T., Chiorboli, C., and Bignozzi, C.A. (1990). Photoinduced

electron and energy transfer in polynuclear complexes. Top. Curr. Chem. *158*, 73–149. 10.1007/3-540-52568-8_3.

48. Strieth-Kalthoff, F., James, M.J., Teders, M., Pitzer, L., and Glorius, F. (2018). Energy transfer catalysis mediated by visible light: principles, applications, directions. Chem. Soc. Rev. *47*, 7190–7202. 10.1016/j.chempr.2019.06.004.

49. Frischmann, P.D., Mahata, K., and Würthner, F. (2013). Powering the future of molecular artificial photosynthesis with light-harvesting metallosupramolecular dye assemblies. Chem. Soc. Rev. *42*, 1847–1870. 10.1039/c2cs35223k.

50. Kimura, E., Wada, S., Shionoya, M., and Okazaki, Y. (1994). New series of multifunctionalized nickel (II)-cyclam (cyclam = 1,4,8,11-tetraazacyclotetradecane) complexes. Application to the Photoreduction of Carbon Dioxide. Inorg. Chem. *33*, 770–778. 10.1021/ic00082a025.

51. Hennessey, S., Farràs, P., Benet-Buchholz, J., and Llobet, A. (2019). A Bpp-based dinuclear ruthenium photocatalyst for visible light-driven oxidation reactions. Catal. Sci. Technol. *9*, 6760–6768. 10.1126/science.1233701.

52. Yamazaki, Y., and Ishitani, O. (2018). Synthesis of Os(II)-Re(i)-Ru(II) hetero-trinuclear complexes and their photophysical properties and photocatalytic abilities. Chem. Sci. *9*, 1031–1041. 10.1039/c7sc04162d.

53. Liu, Y.X., Summers, M.A., Scully, S.R., and McGehee, M.D. (2006). Resonance energy transfer from organic chromophores to fullerene molecules. J. Appl. Phys. *99*, 093251-(1-4). 10.1063/1.2195890.

54. Cerfontaine, S., Wehlin, S.A.M., Elias, B., and Troian-Gautier, L. (2020). Photostable Polynuclear Ruthenium(II) Photosensitizers Competent for Dehalogenation Photoredox

Catalysis at 590 nm. J. Am. Chem. Soc. *142*, 5549–5555. 10.1021/jacs.0c01503.

55. Cerfontaine, S., Troian-Gautier, L., Duez, Q., Cornil, J., Gerbaux, P., and Elias, B. (2021). MLCT Excited-State Behavior of Trinuclear Ruthenium(II) 2,2′-Bipyridine Complexes. Inorg. Chem. *60*, 366–379. 10.1021/acs.inorgchem.0c03004.

56. Ravetz, B.D., Tay, N.E.S., Joe, C.L., Sezen-Edmonds, M., Schmidt, M.A., Tan, Y., Janey, J.M., Eastgate, M.D., and Rovis, T. (2020). Development of a Platform for Near-Infrared Photoredox Catalysis. ACS Cent. Sci. *6*, 2053–2059. 10.1021/acscentsci.0c00948.

57. Thompson, D.W., Ito, A., and Meyer, T.J. (2013). [Ru(bpy)3]2+* and other remarkable metal-to-ligand charge transfer (MLCT) excited states. Pure Appl. Chem. *85*, 1257–1305. 10.1351/PAC-CON-13-03-04.

58. Maurer, A.B., and Meyer, G.J. (2020). Stark Spectroscopic Evidence that a Spin Change Accompanies Light Absorption in Transition Metal Polypyridyl Complexes. J. Am. Chem. Soc. *142*, 6847–6851. 10.1021/jacs.9b13602.

59. Hofbeck, T., and Yersin, H. (2010). The triplet state of fac-Ir(ppy)3. Inorg. Chem. *49*, 9290–9299. 10.1021/ic100872w.

60. Ravetz, B.D., Pun, A.B., Churchill, M., Congreve, D.N., Rovis, T., and Campos, L.M. (2019). Photoredox catalysis using infrared light via triplet fusion upconversion. Nature *565*, 343–346. 10.1038/s41586-018-0835-2.

61. Freitag, M., Möller, N., Rühling, A., Strassert, C.A., Ravoo, B.J., and Glorius, F. (2019). Photocatalysis in the Dark: Near-Infrared Light Driven Photoredox Catalysis by an Upconversion Nanoparticle/Photocatalyst System. ChemPhotoChem *3*, 24–27. 10.1002/cptc.201800212.

62. Huang, L., Wu, W., Li, Y., Huang, K., Zeng, L., Lin, W., and Han, G. (2020). Highly

effective near-infrared activating triplet-triplet annihilation upconversion for photoredox catalysis. J. Am. Chem. Soc. *142*, 18460–18470. 10.1021/jacs.0c06976.

63. Yamazaki, Y., Rohacova, J., Koike, K., and Ishitani, O. (2021). Synthesis and Light-Harvesting Functions of Ring-Shaped Re(I) Trinuclear Complexes Connected with an Emissive Ru(II) Complex. JACS Au *1*, 294–307. 10.1021/jacsau.0c00114.

64. Kent, C.A., Liu, D., Ma, L., Papanikolas, J.M., Meyer, T.J., and Lin, W. (2011). Light Harvesting in Microscale Metal Organic Frameworks by Energy Migration and Interfacial Electron Transfer Quenching. J. Am. Chem. Soc. *133*, 12940–12943. 10.1021/ja204214t.

65. Yamazaki, Y., Rohacova, J., Ohtsu, H., Kawano, M., and Ishitani, O. (2018). Synthesis of Re(I) Rings Comprising Different Re(I) Units and Their Light-Harvesting Abilities. Inorg. Chem. *57*, 15158–15171. 10.1021/acs.inorgchem.8b02421.

66. Mattson, G., Conklin, E., Desai, S., Nielander, G., Savage, M.D., and Morgensen, S. (1993). A Practical Approach to Crosslinking. Mol. Biol. Rep. *17*, 167–183. 10.1007/BF00986726.

67. Mädler, S., Bich, C., Touboul, D., and Zenobi, R. (2009). Chemical cross-linking with NHS esters: A systematic study on amino acid reactivities. J. Mass Spectrom. *44*, 694–706. 10.1002/jms.1544.

68. Isailovic, D., Li, H.W., and Yeung, E.S. (2004). Isolation and characterization of R-phycoerythrin subunits and enzymatic digests. J. Chromatogr. A *1051*, 119–130. 10.1016/j.chroma.2004.07.038.

69. Damrauer, N.H., Cerullo, G., Yeh, A., Boussie, T.R., Shank, C. V., and McCusker, J.K. (1997). Femtosecond dynamics of excited-state evolution in [Ru(bpy)3]2+. Science. *11*, 621–625. 10.1126/science.275.5296.54.

70. Mukuta, T., Tanaka, S., Inagaki, A., Koshihara, S.Y., and Onda, K. (2016). Direct Observation of the Triplet Metal-Centered State in [Ru(bpy)3]2+ Using Time-Resolved Infrared Spectroscopy. ChemistrySelect *1*, 2802–2807. 10.1002/slct.201600747.

71. Tyson, E.L., Niemeyer, Z.L., and Yoon, T.P. (2014). Redox mediators in visible light photocatalysis: Photocatalytic radical thiol-ene additions. J. Org. Chem. *79*, 1427–1436. 10.1021/jo3020825.

72. Gao, X.F., Du, J.J., Liu, Z., and Guo, J. (2016). Visible-Light-Induced Specific Desulfurization of Cysteinyl Peptide and Glycopeptide in Aqueous Solution. Org. Lett. *18*, 1166–1169. 10.1021/acs.orglett.6b00292.

73. Nolan, M.D., and Scanlan, E.M. (2020). Applications of Thiol-Ene Chemistry for Peptide Science. Front. Chem. *8*, 1–21. 10.3389/fchem.2020.583272.

74. Tyson, E.L., Ament, M.S., and Yoon, T.P. (2013). Transition metal photoredox catalysis of radical thiol-ene reactions. J. Org. Chem. *78*, 2046–2050. 10.1021/jo3020825.

75. van Grondelle, R. (1985). Excitation energy transfer, trapping and annihilation in photosynthetic systems. BBA Rev. Bioenerg. *811*, 147–195. 10.1016/0304-4173(85)90017-5.

76. Lindsey, J.S., Taniguchi, M., Bocian, D.F., and Holten, D. (2021). The fluorescence quantum yield parameter in Förster resonance energy transfer (FRET)—Meaning, misperception, and molecular design. Chem. Phys. Rev. *2*, 011302. 10.1063/5.0041132.

77. Lange, J.-P. (2021). Performance metrics for sustainable catalysis in industry. Nat. Catal. *4*, 186–192. 10.1038/s41929-021-00585-2.

78. Mak, C.H., Han, X., Du, M., Kai, J.J., Tsang, K.F., Jia, G., Cheng, K.C., Shen, H.H., and Hsu, H.Y. (2021). Heterogenization of homogeneous photocatalysts utilizing synthetic

and natural support materials. J. Mater. Chem. A *9*, 4454–4504. 10.1039/d0ta08334h.

79. Oi, V.T., Glazer, A.N., and Stryer, L. (1982). Fluorescent Phycobiliprotein Conjugates for Analyses of Cells and Molecules. J. Cell Biol. *93*, 981–986. 10.1083/jcb.93.3.981.

80. Son, M.; Mosquera-Vasquez, S.; Schlau-Cohen, G.S. (2017). Ultrabroadband 2D electronic spectroscopy with high speed, shot-to-shot detection. Opt. Express *25*, 18950–18962. 10.1364/OE.25.018950.